# Langmuir

The ACS Journal of Surfaces and Colloids

DECEMBER 15, 2009
VOLUME 25, NUMBER 24
pubs.acs.org/Langmuir


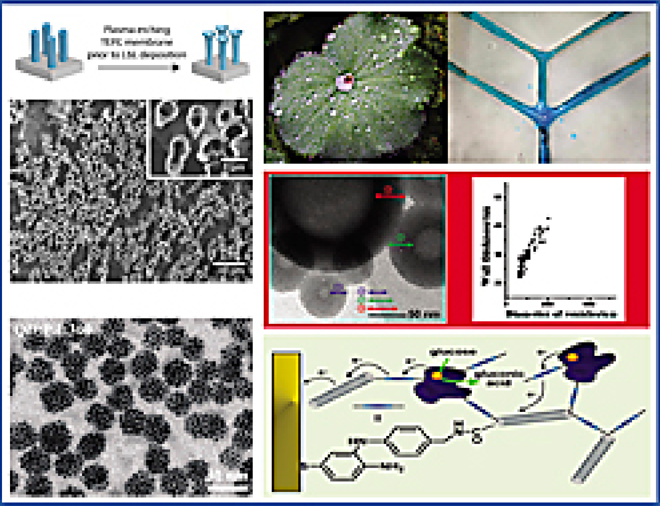

## 25 Years of Langmuir Special Issue

(see p. 9A)

ACS Publications
High quality. High impact.

www.acs.org

# Langmuir

**December 15, 2009**
Volume 25, Issue 24
Pages 13697-14206

Larger Cover



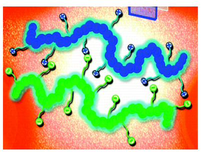



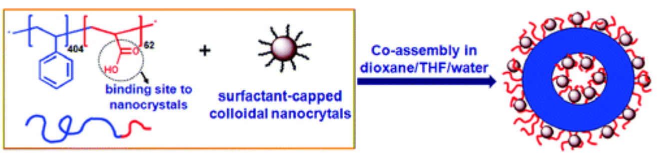

### Not All Anionic Polyelectrolytes Complex with DTAB

Yuguo Cui, Robert Pelton, Terence Cosgrove, Robert Richardson, Sheng Dai, Stuart Prescott, Isabelle Grillo, Howard Ketelson and David Meadows
pp 13712-13717
**Publication Date (Web):** May 26, 2009 (Research Article)
**DOI:** 10.1021/la900563y

Section:
Surface Chemistry and Colloids

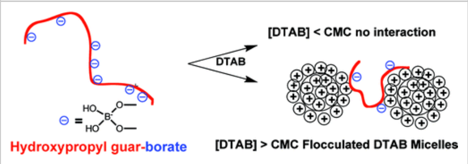


### Multicompartment Micelles from pH-Responsive Miktoarm Star Block Terpolymers

Chun Liu, Marc A. Hillmyer and Timothy P. Lodge
pp 13718-13725
**Publication Date (Web):** May 13, 2009 (Research Article)
**DOI:** 10.1021/la900845u

Section:
Chemistry of Synthetic High Polymers

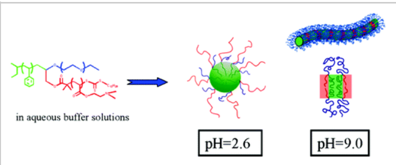


### Oxygen Carrier Based on Hemoglobin/Poly(L-lysine)-*block*-poly(L-phenylalanine) Vesicles

Jing Sun, Yubin Huang, Quan Shi, Xuesi Chen and Xiabin Jing
pp 13726-13729
**Publication Date (Web):** May 21, 2009 (Research Article)
**DOI:** 10.1021/la901194k

Section:
Pharmaceuticals

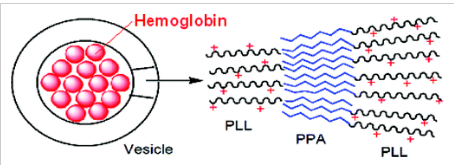


### Relationship between Wall Thickness and Size in Block Copolymer Vesicles

Lie Ma and Adi Eisenberg
pp 13730-13736
**Publication Date (Web):** May 8, 2009 (Research Article)
**DOI:** 10.1021/la9012729

Section:
Physical Properties of Synthetic High Polymers

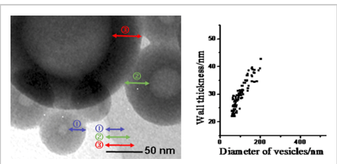

## A New Light-Harvesting Conjugated Polyelectrolyte Microgel for DNA and Enzyme Detections†

**Part of the "Langmuir 25th Year: Molecular and macromolecular self-assemblies" special issue.**

Xuli Feng, Qingling Xu, Libing Liu and Shu Wang

pp 13737-13741
**Publication Date (Web):** June 15, 2009 (Research Article)
**DOI:** 10.1021/la901444c

Section:
Biochemical Methods

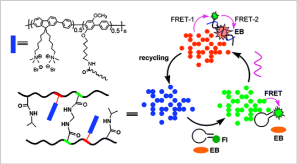

## Insight into the Mechanism of Antimicrobial Poly(phenylene ethynylene) Polyelectrolytes: Interactions with Phosphatidylglycerol Lipid Membranes†

**Langmuir 25th Year: Molecular and macromolecular self-assemblies**

Liping Ding, Eva Y. Chi, Sireesha Chemburu, Eunkyung Ji, Kirk S. Schanze, Gabriel P. Lopez and David G. Whitten

pp 13742-13751
**Publication Date (Web):** June 17, 2009 (Research Article)
**DOI:** 10.1021/la901457t

Section:
General Biochemistry

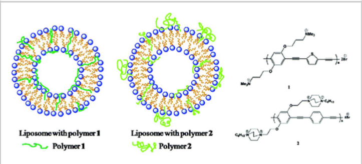

## Nanostructure of a Poly(acrylic acid) Brush and Its Transition in the Amphiphilic Diblock Copolymer Monolayer on the Water Surface

Hideki Matsuoka, Yoshiko Suetomi, Ploysai Kaewsaiha and Kozo Matsumoto

pp 13752-13762
**Publication Date (Web):** July 7, 2009 (Research Article)
**DOI:** 10.1021/la901466h

Section:
Physical Properties of Synthetic High Polymers

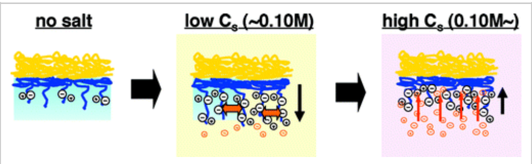


## Electrochemistry of the Inclusion Complexes Formed Between the Cucurbit[7]uril Host and Several Cationic and Neutral Ferrocene Derivatives†

**Part of the "Langmuir 25th Year: Molecular and macromolecular self-assemblies" special issue.**

Lu Cui, Suresh Gadde, Wei Li and Angel E. Kaifer

pp 13763-13769
**Publication Date (Web):** June 22, 2009 (Research Article)
**DOI:** 10.1021/la9015096

Section:
Electrochemistry

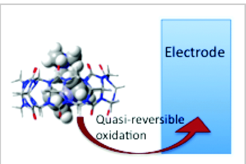

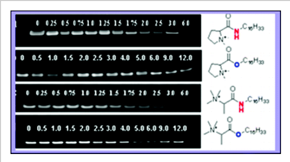



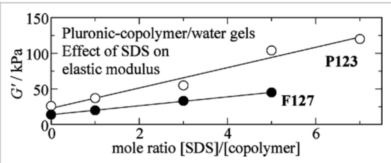
Pluronic-copolymer/water gels
Effect of SDS on
elastic modulus
P123
F127
G' / kPa
150
100
50
0
0
2
4
6
mole ratio [SDS]/[copolymer]



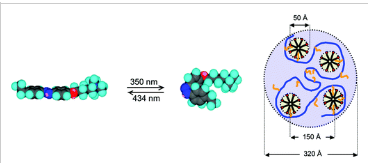
350 nm
434 nm
50 Å
150 Å
320 Å



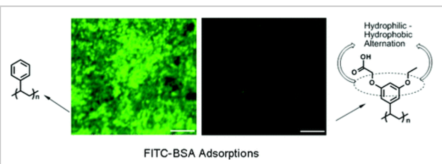
Hydrophilic - Hydrophobic Alternation
FITC-BSA Adsorptions

**Effect of the Structure of Bile Salt Aggregates on the Binding of Aromatic Guests and the Accessibility of Anions**
Rui Li, Eric Carpentier, Edward D. Newell, Lana M. Olague, Eve Heafey, Chang Yihwa and Cornelia Bohne
pp 13800–13808
**Publication Date (Web):** July 16, 2009 (Research Article)
**DOI:** 10.1021/la901826y

Section:
Radiation Chemistry, Photochemistry, and Photographic and Other Reprographic Processes

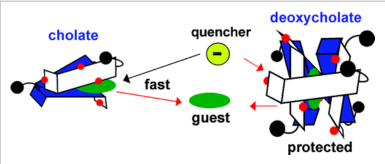


**Internal Composition versus the Mechanical Properties of Polyelectrolyte Multilayer Films: The Influence of Chemical Cross-Linking**
Thomas Boudou, Thomas Crouzier, Rachel Auzély-Velty, Karine Glinel and Catherine Picart
pp 13809–13819
**Publication Date (Web):** September 3, 2009 (Research Article)
**DOI:** 10.1021/la9018663

Section:
Plastics Fabrication and Uses

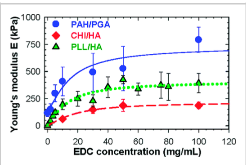


**Self Aggregation of Supramolecules of Nitroxides@Cucurbit[8]uril Revealed by EPR Spectra**
Nithyanandhan Jayaraj, Mintu Porel, M. Francesca Ottaviani, Murthy V. S. N. Maddipatla, Alberto Modelli, José P. Da Silva, Balakrishna R. Bhogala, Burjor Captain, Steffen Jockusch, Nicholas J. Turro and V. Ramamurthy
pp 13820–13832
**Publication Date (Web):** August 14, 2009 (Research Article)
**DOI:** 10.1021/la9020806

Section:
Physical Organic Chemistry

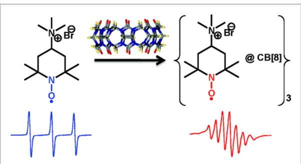


**Dithiocarbamate-Coated SERS Substrates: Sensitivity Gain by Partial Surface Passivation**
Yan Zhao, James N. Newton, Jie Liu and Alexander Wei
pp 13833–13839
**Publication Date (Web):** August 17, 2009 (Research Article)
**DOI:** 10.1021/la902087e

Section:
Organic Analytical Chemistry

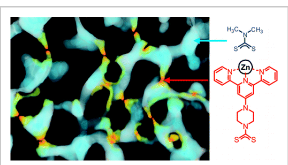

## NANOPARTICLES: SYNTHESIS, PROPERTIES, AND ASSEMBLIES

### Gold Nanoparticles: Past, Present, and Future

Rajesh Sardar, Alison M. Funston, Paul Mulvaney and Royce W. Murray
pp 13840-13851
**Publication Date (Web):** July 2, 2009 (Perspective)
**DOI:** 10.1021/la9019475

Section:
Inorganic Chemicals and Reactions

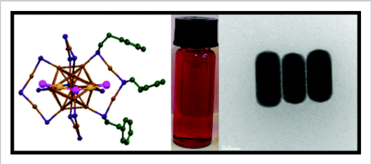

### Formation and Size Tuning of Colloidal Microcapsules via Host−Guest Molecular Recognition at the Liquid−Liquid Interface

Debabrata Patra, Firat Ozdemir, Oscar R. Miranda, Bappaditya Samanta, Amitav Sanyal and Vincent M. Rotello
pp 13852-13854
**Publication Date (Web):** June 18, 2009 (Letter)
**DOI:** 10.1021/la9015756

Section:
Surface Chemistry and Colloids

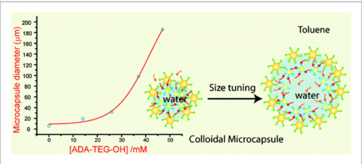


### Monolayer-Protected Gold Nanoparticles Prepared Using Long-Chain Alkanethioacetates

Shishan Zhang, Gyu Leem and T. Randall Lee
pp 13855-13860
**Publication Date (Web):** July 28, 2009 (Letter)
**DOI:** 10.1021/la901847s

Section:
Surface Chemistry and Colloids

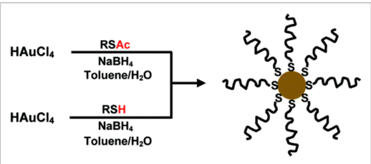


### Self-Assembly of Ligated Gold Nanoparticles: Phenomenological Modeling and Computer Simulations

Siddique J. Khan, F. Pierce, C. M. Sorensen and A. Chakrabarti
pp 13861-13868
**Publication Date (Web):** May 14, 2009 (Research Article)
**DOI:** 10.1021/la9008202

Section:
Surface Chemistry and Colloids

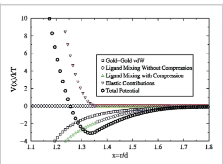

### Graphene−Semiconductor Nanocomposites: Excited-State Interactions between ZnO Nanoparticles and Graphene Oxide
Graeme Williams and Prashant V. Kamat
pp 13869–13873
**Publication Date (Web):** May 19, 2009 (Research Article)
**DOI:** 10.1021/la900905h

Section:
Radiation Chemistry, Photochemistry, and Photographic and Other Reprographic Processes

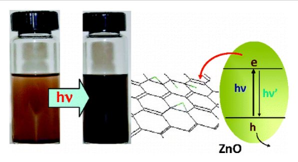


### Gold Nanoparticles with a Polymerizable Surfactant Bilayer: Synthesis, Polymerization, and Stability Evaluation
Alaaldin M. Alkilany and Catherine J. Murphy
pp 13874–13879
**Publication Date (Web):** June 1, 2009 (Research Article)
**DOI:** 10.1021/la901270x

Section:
Surface Active Agents and Detergents

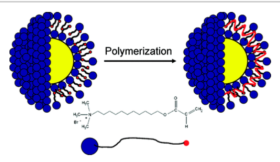


### Metal−Polymer Hybrid Colloidal Particles with an Eccentric Structure
Akira Ohnuma, Eun Chul Cho, Majiong Jiang, Bunsho Ohtani and Younan Xia
pp 13880–13887
**Publication Date (Web):** July 21, 2009 (Research Article)
**DOI:** 10.1021/la9015146

Section:
Surface Chemistry and Colloids

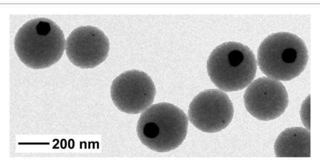


### Photochemical Reactivity of Gold Clusters: Dependence on Size and Spin Multiplicity
Masanori Sakamoto, Takashi Tachikawa, Mamoru Fujitsuka and Tetsuro Majima
pp 13888–13893
**Publication Date (Web):** July 2, 2009 (Research Article)
**DOI:** 10.1021/la901552f

Section:
Radiation Chemistry, Photochemistry, and Photographic and Other Reprographic Processes

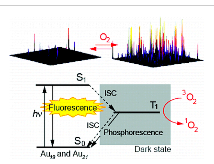

**Highly Controlled Silica Coating of PEG-Capped Metal Nanoparticles and Preparation of SERS-Encoded Particles**
Cristina Fernández-López, Cintia Mateo-Mateo, Ramón A. Álvarez-Puebla, Jorge Pérez-Juste, Isabel Pastoriza-Santos and Luis M. Liz-Marzán
pp 13894–13899
**Publication Date (Web):** July 10, 2009 (Research Article)
**DOI:** 10.1021/la9016454

Section:
Plastics Manufacture and Processing

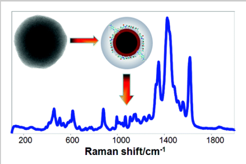


**Coupled Electrochemical/Photochemical Patterning and Erasure of $Ag^0$ Nanoclusters on Au Surfaces**
Michael Riskin and Itamar Willner
pp 13900–13905
**Publication Date (Web):** July 24, 2009 (Research Article)
**DOI:** 10.1021/la901701u

Section:
Radiation Chemistry, Photochemistry, and Photographic and Other Reprographic Processes

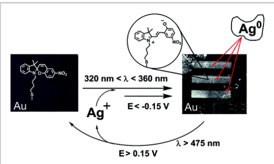


**Highly Stable Biocompatible Inorganic Nanoparticles by Self-Assembly of Triblock-Copolymer Ligands**
Elmar Pöselt, Steffen Fischer, Stephan Foerster and Horst Weller
pp 13906–13913
**Publication Date (Web):** August 11, 2009 (Research Article)
**DOI:** 10.1021/la901876b

Section:
Pharmaceuticals

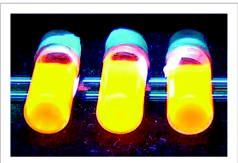

## SELF-ASSEMBLED MONOLAYERS: SYNTHESIS, CHARACTERIZATION, AND APPLICATIONS

**Role of Vapor-Phase Mass Transport During the Spreading of a Long-Chain Alkane Drop**
Lingbo Lu and Yuguang Cai
pp 13914–13917
**Publication Date (Web):** July 6, 2009 (Letter)
**DOI:** 10.1021/la9016917

Section:
Surface Chemistry and Colloids

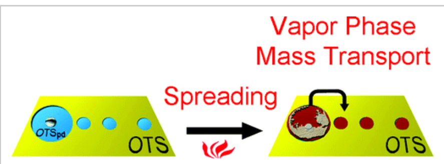

### Headgroup-Dependent Lipid Self-Assembly on Zirconium Phosphate-Terminated Interfaces
B. P. Oberts and G. J. Blanchard
pp 13918-13925
**Publication Date (Web):** May 21, 2009 (Research Article)
**DOI:** 10.1021/la900507w

Section:
General Biochemistry

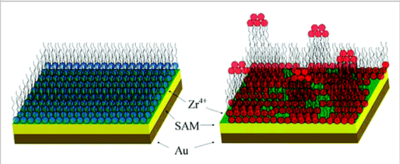


### Assessing the Influence of Adsorbed-State Conformation on the Bioactivity of Adsorbed Enzyme Layers
Kenan P. Fears and Robert A. Latour
pp 13926-13933
**Publication Date (Web):** June 5, 2009 (Research Article)
**DOI:** 10.1021/la900799m

Section:
Enzymes

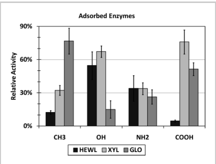


### Comparing the Reactivity of Alkynes and Alkenes on Silicon (100) Surfaces
Albert Ng, Simone Ciampi, Michael James, Jason B. Harper and J. Justin Gooding
pp 13934-13941
**Publication Date (Web):** July 9, 2009 (Research Article)
**DOI:** 10.1021/la901526e

Section:
Surface Chemistry and Colloids

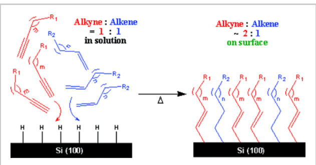


### Using Self-Assembled Monolayers to Model Cell Adhesion to the 9th and 10th Type III Domains of Fibronectin
Jessica L. Eisenberg, Justin L. Piper and Milan Mrksich
pp 13942-13951
**Publication Date (Web):** August 12, 2009 (Research Article)
**DOI:** 10.1021/la901528c

Section:
General Biochemistry

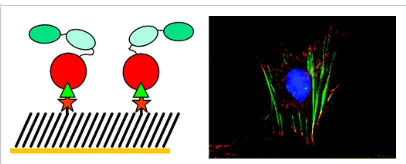

### Site-Specific Immobilization of DNA in Glass Microchannels via Photolithography

TuHa Vong, Jurjen ter Maat, Teris A. van Beek, Barend van Lagen, Marcel Giesbers, Jan C. M. van Hest and Han Zuilhof
pp 13952–13958
**Publication Date (Web):** July 21, 2009 (Research Article)
**DOI:** 10.1021/la901558n

Section:
Biochemical Genetics

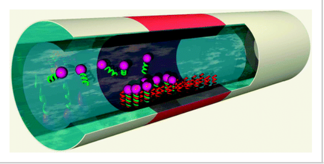

### Long-Chain Alkylthiol Assemblies Containing Buried In-Plane Stabilizing Architectures

Hung-Hsun Lee, Živilė Ruželė, Lyuba Malysheva, Alexander Onipko, Albert Gutés, Fredrik Björefors, Ramu□nas Valiokas and Bo Liedberg
pp 13959–13971
**Publication Date (Web):** September 30, 2009 (Research Article)
**DOI:** 10.1021/la901668u

Section:
Physical Organic Chemistry

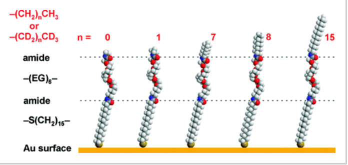


### Porous Multilayer-Coated PDMS Stamps for Protein Printing

Huaping Xu, Alberto Gomez-Casado, Zhihua Liu, David N. Reinhoudt, Rob G. H. Lammertink and Jurriaan Huskens
pp 13972–13977
**Publication Date (Web):** July 13, 2009 (Research Article)
**DOI:** 10.1021/la901797n

Section:
Biochemical Methods

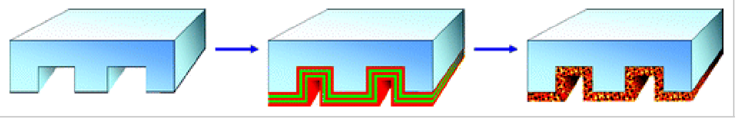

### Electrical Contacting of Redox Enzymes by Means of Oligoaniline-Cross-Linked Enzyme/Carbon Nanotube Composites

Ilina Baravik, Ran Tel-Vered, Oded Ovits and Itamar Willner
pp 13978–13983
**Publication Date (Web):** August 12, 2009 (Research Article)
**DOI:** 10.1021/la902074w

Section:
Biochemical Methods

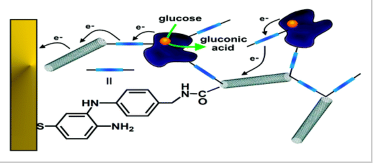

**Patterned Organosilane Monolayers as Lyophobic−Lyophilic Guiding Templates in Surface Self-Assembly: Monolayer Self-Assembly versus Wetting-Driven Self-Assembly**


Section:
Surface Chemistry and Colloids

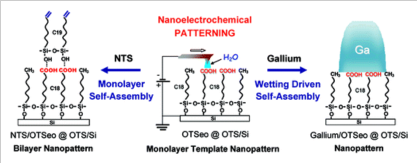


**Crystallization of Malonic and Succinic Acids on SAMs: Toward the General Mechanism of Oriented Nucleation on Organic Monolayers**


Section:
Surface Chemistry and Colloids

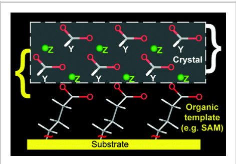


## SELF-ASSEMBLED POLYELECTROLYTE MULTILAYERS: STRUCTURE AND FUNCTION

**Retrospective on the Future of Polyelectrolyte Multilayers**


Section:
Physical Properties of Synthetic High Polymers

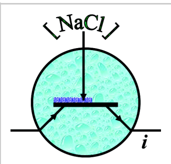


**Encapsulation of Bacterial Spores in Nanoorganized Polyelectrolyte Shells**


Section:
Pharmaceuticals

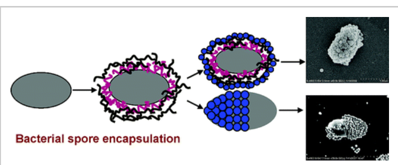

**Spin-Assisted Layer-by-Layer Assembly: Variation of Stratification as Studied with Neutron Reflectivity**
Eugenia Kharlampieva, Veronika Kozlovskaya, Jennifer Chan, John F. Ankner and Vladimir V. Tsukruk
pp 14017–14024
**Publication Date (Web):** July 6, 2009 (Research Article)
**DOI:** 10.1021/la9014042

Section:
Surface Chemistry and Colloids

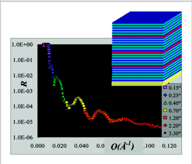

**Hydrogen-Bonded Layer-by-Layer Temperature-Triggered Release Films**
Aliaksandr Zhuk, Svetlana Pavlukhina and Svetlana A. Sukhishvili
pp 14025–14029
**Publication Date (Web):** July 2, 2009 (Research Article)
**DOI:** 10.1021/la901478v

Section:
Plastics Fabrication and Uses

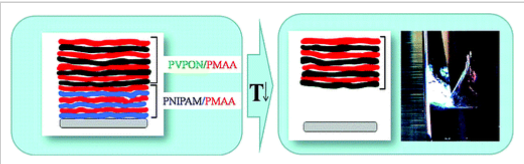


**Tunable Synthesis of Prussian Blue in Exponentially Growing Polyelectrolyte Multilayer Films**
Nicolas Laugel, Fouzia Boulmedais, Alae E. El Haitami, Pierre Rabu, Guillaume Rogez, Jean-Claude Voegel, Pierre Schaaf and Vincent Ball
pp 14030–14036
**Publication Date (Web):** August 13, 2009 (Research Article)
**DOI:** 10.1021/la901479z

Section:
Coatings, Inks, and Related Products

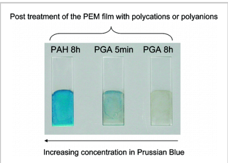


**Surface-Supported Multilayers Decorated with Bio-active Material Aimed at Light-Triggered Drug Delivery**
D. V. Volodkin, N. Madaboosi, J. Blacklock, A. G. Skirtach and H. Möhwald
pp 14037–14043
**Publication Date (Web):** August 11, 2009 (Research Article)
**DOI:** 10.1021/la9015433

Section:
Pharmaceuticals

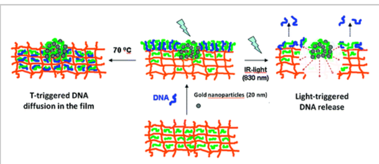

### pH-Responsive Reversibly Swellable Nanotube Arrays
Khek-Khiang Chia, Michael F. Rubner and Robert E. Cohen
pp 14044-14052
**Publication Date (Web):** July 9, 2009 (Research Article)
**DOI:** 10.1021/la9015959

Section:
Plastics Manufacture and Processing

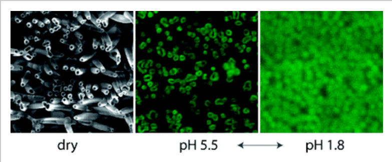


### Luminescent Metal Complexes within Polyelectrolyte Layers: Tuning Electron and Energy Transfer
Lynn Dennany, Gordon G. Wallace and Robert J. Forster
pp 14053-14060
**Publication Date (Web):** July 14, 2009 (Research Article)
**DOI:** 10.1021/la901661v

Section:
Electrochemistry

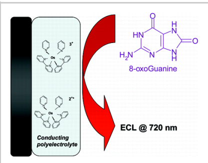


### Specific Ion versus Electrostatic Effects on the Construction of Polyelectrolyte Multilayers
John E. Wong, Heidemarie Zastrow, Werner Jaeger and Regine von Klitzing
pp 14061-14070
**Publication Date (Web):** August 25, 2009 (Research Article)
**DOI:** 10.1021/la901673u

Section:
Plastics Manufacture and Processing

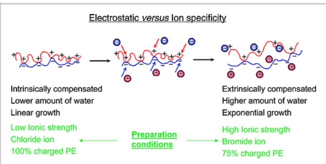


### Silencing Red Blood Cell Recognition toward Anti-A Antibody by Means of Polyelectrolyte Layer-by-Layer Assembly in a Two-Dimensional Model System
Sania Mansouri, Julien Fatisson, Zhimei Miao, Yahye Merhi, Françoise M. Winnik and Maryam Tabrizian
pp 14071-14078
**Publication Date (Web):** August 24, 2009 (Research Article)
**DOI:** 10.1021/la9016799

Section:
Pharmaceuticals

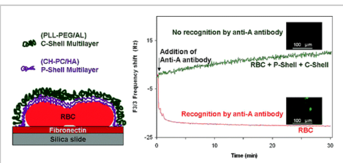

### Tuning the Formation and Degradation of Layer-by-Layer Assembled Polymer Hydrogel Microcapsules

Alisa L. Becker, Alexander N. Zelikin, Angus P. R. Johnston and Frank Caruso

pp 14079-14085
**Publication Date (Web):** July 6, 2009 (Research Article)
**DOI:** 10.1021/la901687a

Section:
Pharmaceuticals

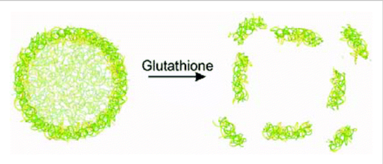


### MAD (Multiagent Delivery) Nanolayer: Delivering Multiple Therapeutics from Hierarchically Assembled Surface Coatings

Byeong-Su Kim, Renée C. Smith, Zhiyong Poon and Paula T. Hammond

pp 14086-14092
**Publication Date (Web):** July 24, 2009 (Research Article)
**DOI:** 10.1021/la9017618

Section:
Pharmaceuticals

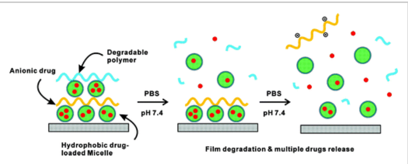


### Highly Ductile Multilayered Films by Layer-by-Layer Assembly of Oppositely Charged Polyurethanes for Biomedical Applications

Paul Podsiadlo, Ming Qin, Meghan Cuddihy, Jian Zhu, Kevin Critchley, Eugene Kheng, Amit K. Kaushik, Ying Qi, Hyoung-Sug Kim, Si-Tae Noh, Ellen M. Arruda, Anthony M. Waas and Nicholas A. Kotov

pp 14093-14099
**Publication Date (Web):** October 13, 2009 (Research Article)
**DOI:** 10.1021/la9021323

Section:
Pharmaceuticals

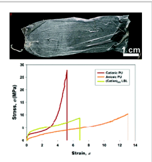


## WETTING AND SUPERHYDROPHOBICITY

### Wetting and Superhydrophobicity

Lichao Gao and Thomas J. McCarthy, Xi Zhang

pp 14100-14104
**Publication Date (Web):** September 22, 2009 (Perspective)
**DOI:** 10.1021/la903043a

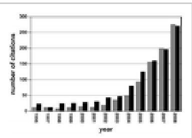



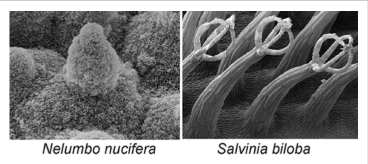
*Nelumbo nucifera*
*Salvinia biloba*



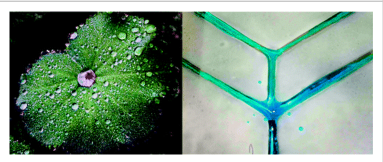



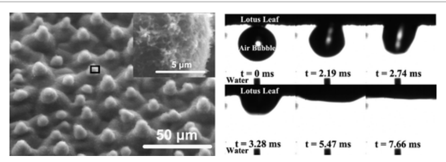

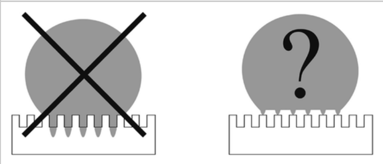



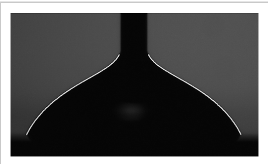



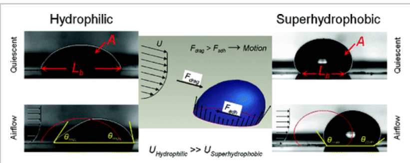
Hydrophilic
Superhydrophobic



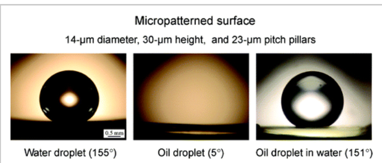
Micropatterned surface
14-μm diameter, 30-μm height, and 23-μm pitch pillars
Water droplet (155°)
Oil droplet (5°)
Oil droplet in water (151°)

**Surfactant-Enhanced Rapid Spreading of Drops on Solid Surfaces**
D. R. Beacham and O. K. Matar, R. V. Craster
pp 14174-14181
**Publication Date (Web):** September 4, 2009 (Research Article)
**DOI:** 10.1021/la9019469

Section:
Surface Chemistry and Colloids

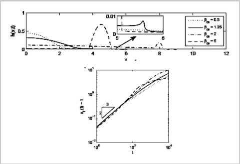

**Sliding of Water Droplets on the Superhydrophobic Surface with ZnO Nanorods†**
**Part of the “Langmuir 25th Year: Wetting and superhydrophobicity” special issue.**
Munetoshi Sakai, Hiroki Kono, Akira Nakajima, Xintong Zhang, Hideki Sakai, Masahiko Abe and Akira Fujishima
pp 14182-14186
**Publication Date (Web):** June 15, 2009 (Research Article)
**DOI:** 10.1021/la901461k

Section:
Surface Chemistry and Colloids

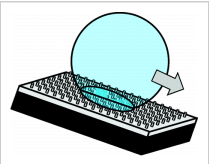

**Preparation of Superhydrophobic Surfaces of Hierarchical Structure of Hybrid from Nanoparticles and Regular Pillar-Like Pattern†**
**Part of the "Langmuir 25th Year: Wetting and superhydrophobicity" special issue.**
Kuan-Yu Yeh, Kuan-Hung Cho and Li-Jen Chen
pp 14187-14194
**Publication Date (Web):** June 19, 2009 (Research Article)
**DOI:** 10.1021/la9015492

Section:
Surface Chemistry and Colloids

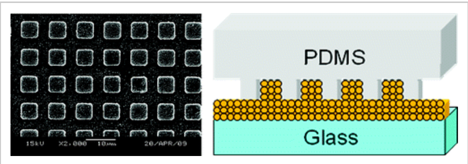


**“Dual-Parallel-Channel” Shape-Gradient Surfaces: Toward Oriented and Reversible Movement of Water Droplets**
Jilin Zhang and Yanchun Han
pp 14195-14199
**Publication Date (Web):** August 17, 2009 (Research Article)
**DOI:** 10.1021/la9014898

Section:
Unit Operations and Processes

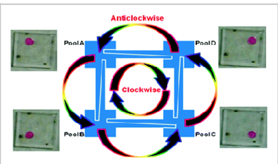

**Reactive Surface Coatings Based on Polysilsesquioxanes: Defined Adjustment of Surface Wettability**

Daniel Kessler and Patrick Theato

pp 14200–14206
**Publication Date (Web):** April 16, 2009 (Research Article)
**DOI:** 10.1021/la9005949

Section:

Chemistry of Synthetic High Polymers

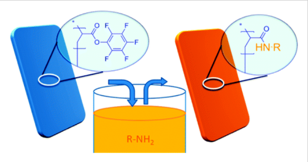

Langmuir
Article
pubs.acs.org/Langmuir


# Air Bubble Bursting Effect of Lotus Leaf[†]

Jingming Wang,[‡] Yongmei Zheng,[‡] Fu-Qiang Nie,[§] Jin Zhai,[§] and Lei Jiang*,[‡,§]

[‡]*School of Chemistry and Environment, Beihang University, Beijing 100191, P. R. China, and* [§]*Beijing National Laboratory for Molecular Sciences, Key Laboratory of Organic Solids, Institute of Chemistry, Chinese Academy of Sciences, Beijing 100190, P. R. China*

*Received March 30, 2009. Revised Manuscript Received May 28, 2009*

In this paper, a phenomenon of air bubbles quickly bursting within several milliseconds on a "self-cleaning" lotus leaf was described. This observation prompted the synthesis of artificial surfaces similar to that of the lotus leaf. The artificial leaf surfaces, prepared by photolithography and wet etching, showed a similar air bubble bursting effect. Smooth and rough silicon surfaces with an ordered nanostructure or patterned microstructure were utilized to study the contribution of the micro/nano hierarchical structures to this phenomenon of air bubble bursting. Air bubbles were found to burst on some superhydrophobic surfaces with microstructure (within 220 ms). However, air bubbles burst much more rapidly (within 13 ms) on similar surfaces with micro/nanostructure. The height, width, and spacing of hierarchical structures could also affect air bubble bursting, and the effect of the height was more obvious. When the height of hierarchical structures was around the height found in natural lotus papillae, the width and spacing were significant for air bubble bursting. An original model was proposed to further evaluate the reason why the micro/nano hierarchical rough structures had an excellent air bubble bursting effect, and the validity of the model was theoretically demonstrated.

## Introduction

Many surfaces in nature, such as various plant leaves,[1,2] water strider's legs,[3] desert beetle's backs,[4] and butterfly's wings,[5] exhibit amazing superhydrophobicity, which has been called the "self-cleaning" property, i.e., water droplets can form nearly perfect spheres on these surfaces and readily roll off the surfaces, picking up and removing surface contaminants as they roll. Numerous studies have revealed that this superhydrophobicity is attributable to a combination of surface chemistry and rough structures of the lotus leaf surface.[6−10] Inspired by nature, artificial superhydrophobic surfaces have now been constructed and explored, as self-cleaning and nonwettable surfaces have immense importance in fundamental research and abundant potential applications.[11−16] To date, most of the research effort has been devoted to investigating superhydrophobic surfaces in air rather than in a water environment. In fact, the dewetting properties of hydrophobic surfaces have many equally important uses in a water environment, being crucial to the recovery of coal and valuable minerals from ores,[17] in wastewater treatment,[18] and in the de-inking of waste paper.[19] However, in order for these processes to be carried out, the hydrophobic surfaces must combine with surfactants to allow effective separation, because the behavior of the liquid film between air bubbles and hydrophobic surfaces can be greatly affected by surfactants.[20,21] Not surprisingly, therefore, the interaction between hydrophobic surfaces and air bubbles in a water environment has been intensively studied in recent years, including phenomena such as collisions,[22,23] attachment,[24−26] and three-phase contact line (TPCL) formation and movement.[27,28] However, to the best of our knowledge, the behavior of the air bubble itself on a superhydrophobic surface in a water environment has not yet been documented.

In this study, the behavior of an air bubble bursting on a lotus leaf surface, a well-known natural superhydrophobic surface, was first investigated. An air bubble was found to spread completely on the superhydrophobic lotus leaf. This spread was rapid, due to the leaf surface's special hierarchical rough structures of micropapillae and nanowax crystals. We were also able to reproduce this effect on an "artificial lotus leaf", i.e., a superhydrophobic silicon surface, with similar hierarchical rough structures. These results open

[†] Part of the "Langmuir 25th Year: Wetting and superhydrophobicity" special issue.

*To whom correspondence should be addressed. School of Chemistry and Environment, Beihang University, Beijing 100191, P. R. China; Key Laboratory of Organic Solids, Institute of Chemistry, Chinese Academy of Sciences, Beijing 100190, P. R. China; E-mail address: jianglei@iccas.ac.cn; Tel.: +86 10 82621396; Fax: +86 10 82627566.

(1) Barthlott, W.; Neinhuis, C. *Planta* **1997**, *202*, 1.
(2) Herminghaus, S. *Europhys. Lett.* **2000**, *52*, 165.
(3) Gao, X.; Jiang, L. *Nature* **2004**, *432*, 36.
(4) Parker, A. R.; Lawrence, C. R. *Nature* **2001**, *414*, 33.
(5) Zheng, Y. M.; Gao, X. F.; Jiang, L. *Soft Mat.* **2007**, *3*, 178.
(6) Wenzel, R. N. *Ind. Eng. Chem.* **1936**, *28*, 988.
(7) Cassie, A. B. D.; Baxter, S. *Trans. Faraday Soc.* **1944**, *40*, 546.
(8) Callies, M.; Quéré, D. *Soft Mat.* **2005**, *1*, 55.
(9) Marmur, A. *Langmuir* **2003**, *19*, 8343.
(10) Nosonovsky, M. *Langmuir* **2007**, *23*, 3157.
(11) Blossey, R. *Nat. Mater.* **2003**, *2*, 301.
(12) Xie, Q.; Xu, J.; Fen, L.; Jiang, L.; Tang, W.; Luo, X.; Han, C. C. *Adv. Mater.* **2004**, *16*, 302.
(13) Shirtcliffe, N. J.; McHale, G.; Newton, M. I.; Chabrol, G.; Perry, C. C. *Adv. Mater.* **2004**, *16*, 1929.
(14) Shi, F.; Wang, Z. Q.; Zhang, X. *Adv. Mater.* **2005**, *17*, 1005.
(15) Nakajima, A.; Hashimoto, K.; Watanabe, T. *Monatsh. Chem.* **2001**, *132*, 31.
(16) Quéré, D. *Rep. Prog. Phys.* **2005**, *68*, 2495.
(17) Fuerstenau, D. W.; Herrera-Urbina, R. *Surfactant Sci. Ser.* **1989**, *33*, 259.
(18) Odegaard, H. *Water Sci. Technol.* **2001**, *43*, 75.
(19) Drelich, J.; Miller, J. D. *Prog. Paper Recyc.* **2001**, *11*, 38.
(20) Shen, H.; Pugh, R .J.; Forssberg, E. *Colloid Surf., A* **2002**, *196*, 63.
(21) Wang, G.; Pelton, R.; Hrymak, A.; Shawafaty, N.; Heng, Y. M. *Langmuir* **1999**, *15*, 2202.
(22) Krasowska, M.; Krastev, R.; Rogalski, M.; Malysa, K. *Langmuir* **2007**, *23*, 549.
(23) Li, D.; Liu, S. *Langmuir* **1996**, *12*, 5216.
(24) Fan, X.; Zhang, Z.; Li, G.; Rowson, N. A. *Chem. Eng. Sci.* **2004**, *59*, 2639.
(25) Wang, W.; Zhou, Z.; Nandakumar, K.; Masliyah, J. H.; Xu, Z. *Int. J. Miner. Process.* **2005**, *75*, 69.
(26) Kralchevsky, P. A. *Langmuir* **1996**, *12*, 5951.
(27) Mukherjee, M.; Lahiri, A. K. *J. Colloid Interface Sci.* **2005**, *291*, 593.
(28) Deschenes, L. A.; Zilaro, P.; Muller, L. J.; Fourkas, J. T.; Mohanty, U. *J. Phys. Chem. B* **1997**, *101*, 5777.

a new avenue for applied industrial separation processes but also benefit basic research into bubble-related interfacial phenomena.

## Experimental Section

**Sample Preparation.** Lotus leaves were freshly obtained from a pond in Beijing, China. Samples of lotus leaves were cut into square pieces sized about 10 × 10 $mm^2$, avoiding the veins. Silicon wafers 4 in diameter were obtained from Organic Metal Academe (100 orientation, Beijing). An ordered array of micropillar structures was fabricated using photolithography, as follows. A contact lithographic mask was obtained from the Institute of Microelectronics of the Chinese Academy of Sciences (Beijing, China). The mask aligner/exposure system (Karl Suss MA6, Germany) was used to transfer the micropatterns of the mask onto silicon wafers. The deep etching process was completed using an etch system (STS ICP ASE, U.K.). An ordered array of nanowire structures on smooth surfaces was fabricated through a wet etching process.[29] Clean silicon wafers were immersed in a Teflon-lined stainless steel autoclave with etching solution containing 15 mL HF, 35 mL deionized water, and 0.1699 g $AgNO_3$ for 5 to 10 min at 50 °C. After the etching progress, the wafers were dipped into $HNO_3$ for a few seconds until the upper white film disappeared. The wafers were then rinsed with deionized water and blown dry with nitrogen. For the fabrication of an "artificial lotus leaf" surface, two processes were adopted according to a statistical analysis of the dimension and distribution of lotus papillae. The first step was to fabricate an ordered array of micropillar structures by photolithography. Wet etching was then utilized to form a microcone array. In order to obtain silicon surfaces with superhydrophobicity, the patterned silicon substrates were immersed into a 1.0 wt % ethanol solution of hydrolyzed FAS-17 (Shin-Etsu Chemical Co., Ltd., Tokyo, Japan) for 10 h at room temperature and then dried in an oven at 140 °C for 1 h.

**Measurement.** The surface structures of the lotus leaf were characterized using an environmental SEM apparatus (HITACHI S-3000N, Japan) at 5 °C under low-vacuum mode. SEM images of superhydrophobic silicon surfaces with different structures were taken in a field emission SEM apparatus (JEOL JSM-6700F, Japan) operated at 3.0 kV. Schematics of the experimental setup constructed to study the behavior of an air bubble on these surfaces is shown in Figure 1a. A square quartz cell (20 × 20 × 20 $mm^3$) filled with water was fixed onto the Dataphysics OCA20 system (Optical Contact Angle Measurement), and the samples were positioned horizontally in the water at a depth of about 3 mm. All of the samples were immersed in the experimental apparatus for 30 min before testing to achieve a redistributed, well-proportioned air layer in water. Air bubbles were released from a bent needle (outer-Φ, 0.52 mm; inner-Φ, 0.26 mm; length, 57 mm; width, 15 mm; upward, 7 mm). Air bubbles could leave the needle orifice when the injection speed was greater than 10 $\mu$L/s. The volume of the exiting air bubble was about 3 $\mu$L, and the distance between the sample surface and the needle orifice was fixed at about 3 mm.

The bubble contact angle (CA) was measured by the captive bubble method (OCA20, Dataphysics Inc., Germany) and was used as a quantitative parameter to investigate air bubble bursting behavior on different surfaces. Here, the bubble CA illustrated in Figure 1b is defined as the observed equilibrium CA of liquid around the pinned bubbles on a solid surface, where the liquid/air interface meets the solid/liquid interface across the three phase contact interfaces. The behavior of air bubbles on different surfaces was investigated by a high-speed camera (HCC1000F, VDS Vosskühler GmbH, Germany) with maximum of 1892 frames/s, and recording time was calculated by the frame frequency and number.

(29) Peng, K. Q.; Yan, Y. J.; Gao, S. P.; Zhu, J. *Adv. Mater.* **2002**, *14*, 1164.

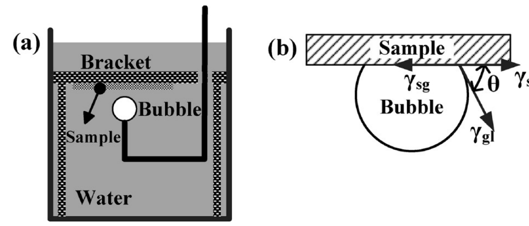


**Figure 1.** Experimental setup and measurement of the air bubble contact angle ($\theta$). (a) Schematic illustration of the experimental setup. (b) Schematic illustration of the air bubble contact angle (CA), which was measured by the captive bubble method.

## Results and Discussion

First, the behavior of air bubble on lotus leaf surface was investigated, as illustrated in Figure 2. From the typical large-scale environmental SEM image in Figure 2a, numerous papillae can be seen on the lotus leaf surface; these occurred in a random distribution at a calculated density of 2000−3000 per $mm^2$. On the whole, the height and bottom diameter of papillae are 12−15 $\mu$m and 7−10 $\mu$m, respectively. The inset of Figure 2a shows higher resolution of a single papilla, where the nanobranch-like crystals with a diameter of 100−150 nm can be clearly observed. The micropapillae and the nanobranch-like hydrophobic wax crystals together comprise the so-called micro/nano hierarchical rough structures of the lotus leaf surface.

A high-speed camera was then utilized to take a series of optical images. These clearly depicted the dynamic spreading process of the air bubble, as shown in Figure 2b. As the air bubble rose and just contacted the lotus leaf surface (i.e., $t = 0$), it was nearly spherical. However, the contact area between air bubble and lotus leaf surface immediately expanded, and the air bubble's shape changed until it had completely spread out over the lotus leaf surface. At this point, the bubble CA was 179.8 ± 1.7°. We have defined this complete spreading-out process on the lotus leaf surface as "air bubble bursting". On the basis of repeat experiments, the burst time ($\tau$) was within 8 ms.

After viewing this novel phenomenon of an air bubble rapidly and completely bursting on a lotus leaf surface, an "artificial lotus leaf" with similar micro/nanohierarchical structures on a silicon surface was developed. For this, we used the statistical results of lotus papillae dimension and distribution[30] and then modified with a heptadecafluorodecyltrimethoxysilane (FAS-17, $CF_3(CF_2)_7CH_2CH_2{-}Si(OCH_3)_3$) monolayer to endow the surface with a "self-cleaning" property.[31] The behavior of an air bubble on this surface is shown in Figure 3. SEM images of the silicon surface in Figure 3a indicate that "artificial lotus leaf" consists of a uniform microcone array similar to papillae with height of ∼14.5 $\mu$m, a bottom width of ∼9.5 $\mu$m, and spacing between two adjacent microcones of ∼10.2 $\mu$m. Furthermore, the magnification of a microcone (see the inset of Figure 3a) reveals many silicon nanoparticle clusters (width 100−200 nm), which are similar to the nanobranch-like wax crystals of the lotus leaf. The series of optical images in Figure 3b were taken to study the air bubble bursting process on the "artificial lotus leaf" surface.

(30) By examining lotus leaves with an ESEM, the hierarchical rough structures of lotus leaf were counted, and it was found that the diameter of nanobranch-like crystals which were seen covering both at bottom of lotus leaf surface and on micropapillae was about 100−150 nm, and the papillae on lotus leaf were composed of height 12−15 $\mu$m, bottom diameter 7−10 $\mu$m, and number per $mm^2$ of 2000−3000. If it was assumed that lotus papillae showed normal distribution, papilla matrix per $mm^2$ was between 45 × 45 and 55 × 55, and the spacing of papillae was calculated in the range 5−12 $\mu$m.

(31) Nishino, T.; Meguro, M.; Matsushita, K.; Ueda, Y. *Langmuir* **1999**, *15*, 4321.

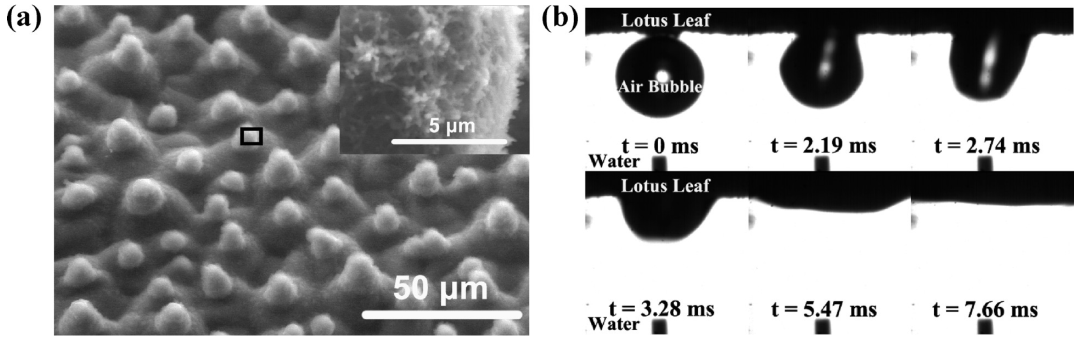


**Figure 2.** SEM images of the lotus leaf surface and optical images showing the air bubble bursting process. (a) SEM images of a lotus leaf surface showing the hierarchical rough structures (inset: a high-resolution image of nanobranch-like wax crystals). (b) A series of optical images showing the bursting process of a rising air bubble, where the time that the air bubble just contacted the lotus leaf surface before deformation was taken as the starting point, i.e., $t = 0$.

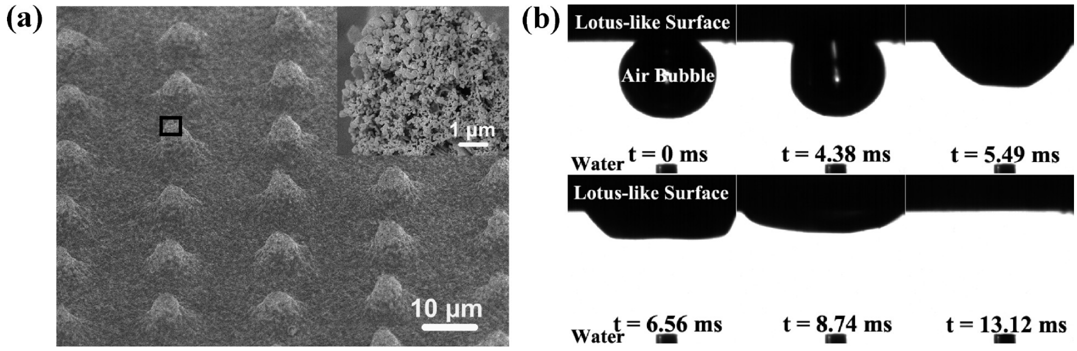


**Figure 3.** SEM images of the "artificial lotus leaf" and air bubble bursting behavior on its surface. (a) The uniform microcone array (inset: high-resolution image of nanoparticle clusters (100−200 nm wide)). The height, bottom diameter, and spacing were about 14.5, 9.5, and 10.2 $\mu$m, respectively. (b) A series of optical images showing the air bubble bursting process on the "artificial lotus leaf" surface.

Air bubbles went through a similar bursting process as they did on the natural lotus leaf and ultimately burst within 13 ms (bubble CA was 174.8 ± 1.5°).

Micro/nano hierarchical rough structures composed of micropapillae and nanobranch-like hydrophobic wax crystals on lotus leaf surface provide it with the perfect "self-cleaning" effect.[32,33] The effects of hierarchical rough structures on air bubble bursting were investigated by observing air bubble behavior on hydrophobic smooth silicon surfaces modified with a FAS-17 monolayer (the average water CA of 112.7 ± 8.5°) as shown in Figure 4. When an air bubble collided with this smooth surface, it did not spread but bounced backward. The air bubble shape would keep changing; then after several "collision−bounce" cycles, a steady TPCL would finally form, i.e., the air bubble would "pin" itself to the smooth surface (with bubble CA of 67.1 ± 6.5°) rather than bursting. This whole scenario would take about 87 ms. These results indicated that the hierarchical rough structures were very important to the air bubble bursting effect.

To further understand the contribution of the hierarchical rough structures on air bubble bursting, silicon surfaces with ordered nanostructure or patterned microstructure were fabricated. SEM images of a nanowire array and a micropillar array are shown in Figure 5a,b, respectively. The width and height of the nanowires are 150−200 nm and about 4.3 $\mu$m, respectively (Figure 5a). The width and height of the micropillars on smooth surfaces are about 9.8 and 14.5 $\mu$m, respectively, and spacing between two adjacent micropillars is about 10.1 $\mu$m (Figure 5b). The series of optical images in Figure 5a′ and b′ describe the air bubble behavior on the nanowire array or micropillar array. When a rising air bubble contacted the nanowire array, the air bubble immediately "pinned" the surface with a bubble CA of 57.8 ± 8.5° and spread very little. This state of the air bubble did not change with time, which meant that this air bubble would not burst. In contrast, an air bubble was able to spread on the micropillar array that had a similar size distribution as micropapillae of lotus leaf, on which bubble CA was 172.3 ± 4.5°. However, the burst time on the micropillar array ($\tau_{\text{micro}} \approx 220$ ms) was much greater than on the "artificial lotus leaf" ($\tau_{\text{artifial}} \approx 13$ ms) and on the lotus leaf surface ($\tau_{\text{lotus}} \approx 8$ ms). These results demonstrated that singly neither the micro nor nanostructure was effective in causing the air bubble bursting phenomenon to occur.

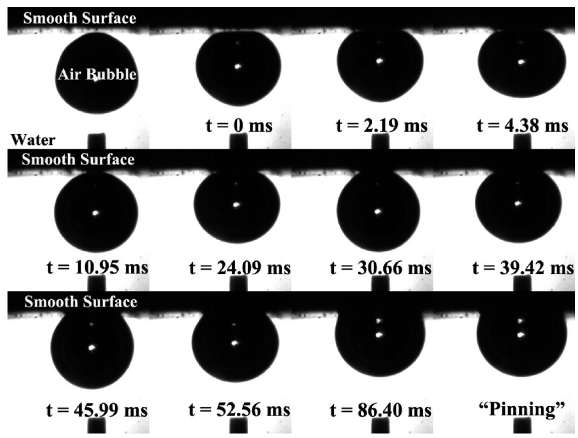


**Figure 4.** A series of optical images showing air bubble behavior on smooth silicon surface.

(32) Feng, L.; Li, S.; Li, H.; Zhang, L.; Zhai, J.; Song, Y.; Liu, B.; Jiang, L.; Zhu, D. *Adv. Mater*. **2002**, *14*, 1857.
(33) Cheng, Y.; Rodak, D.; Wong, C.; Hayden, C. *Nanotechnology* **2006**, *17*, 1359.

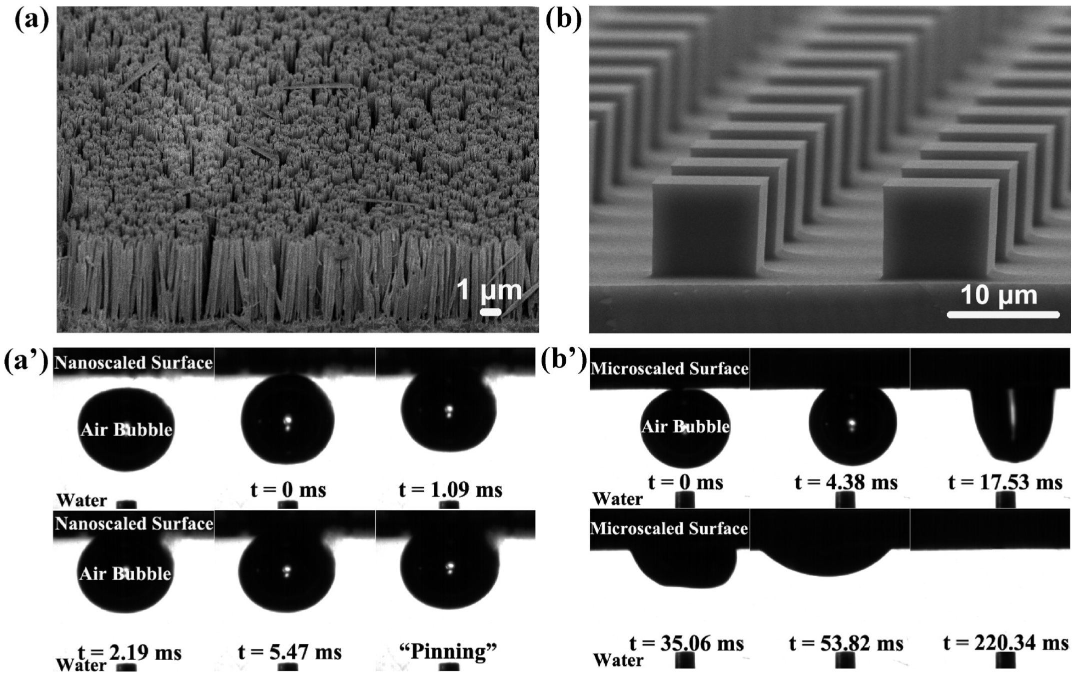


**Figure 5.** SEM images of single-scaled rough structure on silicon surfaces and air bubble behavior on surfaces. (a) Side view of large-area ordered nanowire array on silicon wafers. The width and height of nanowires were 150−200 nm and about 4.3 μm, respectively. (a′) A series of optical images showing air bubble behavior on the nanowire array depicted in (a). (b) Side view of patterned micropillar array. The width and height of the micropillars with the smooth surfaces were about 9.8 and 14.5 μm, respectively, and the spacing between two adjacent micropillars was 10.1 μm. (b′) A series of optical images showing the air bubble bursting process on micropillar arrays in (b).

**Table 1. Air Bubble CA with Different Size Parameters (Height, Bottom Width, and Spacing)[a]**

| Bubble CA (°) / Width (μm) | Height (μm) / Spacing (μm) | 5.0 | 14.5 | 40.0 |
|---|---|---|---|---|
| 3.4 | 19.7 | 35.4±8.9 | 62.8±4.6 | |
| 2.4 | 16.8 | 26.2±7.6 | 98.1±3.8 | |
| 2.7 | 14.5 | 35.2±10.4 | 54.9±4.2 | |
| 4.6 | 18.3 | 29.6±7.7 | 60.5±4.3 | 150.1±2.8 |
| 5.6 | 13.7 | 34.5±4.6 | 155.5±3.2 | 153.8±3.2 |
| 5.3 | 11.3 | 27.4±5.1 | 157.0±3.4 | 157.7±1.2 |
| 8.33 | 14.2 | 73.5±3.2 | 161.4±2.4 | 161.9±1.7 |
| 9.6 | 9.7 | 93.7±2.6 | *174.8*±1.2 | *175.2*±1.5 |
| 9.2 | 6.8 | 78.2±2.1 | 150.5±1.2 | 151.2±3.2 |
| 12.8 | 10.5 | 38.0±4.5 | 55.7±6.3 | 154.4±2.4 |
| 12.6 | 7.2 | 32.4±7.2 | 62.8±5.2 | 154.4±2.0 |
| 12.2 | 4.3 | 50.3±6.1 | 52.0±4.9 | 131.0±3.8 |

[a] Here, the bubble CAs observed are equilibrium CAs, used as quantitative parameters to investigate air bubble bursting behavior on different surfaces. Note that the air bubble CAs illustrated in the panes of solid line are more than 150°. Especially at the height of 14.5 and 40.0 μm, the air bubble CAs can reach more than 170° (in the pane of dashed line) when the width and spacing are about 10 μm.

In addition, because the size and distribution of the microstructure is believed to affect the wetting/dewetting property of superhydrophobic surfaces,[34,35] the effects of height, width, and spacing of the microcone array on air bubble behavior were further investigated, as shown in Table 1. In this case, bubble CA was adopted as the quantitative parameter for studying the bubble behavior on different surfaces. It was considered that an air bubble had adequately spread if the bubble CA was more than 170°. In Table 1, the cases with more than 150° bubble CA are indicated using solid panes, while

(34) Sbragaglia, M.; Peters, A. M.; Pirat, C.; Borkent, B. M.; Lammertink, R. G. H.; Wessling, M.; Lohse, D. *Phys. Rev. Lett.* **2007**, *99*, 156001.
(35) Oner, D.; McCarthy, T. J. *Langmuir* **2000**, *16*, 7777.

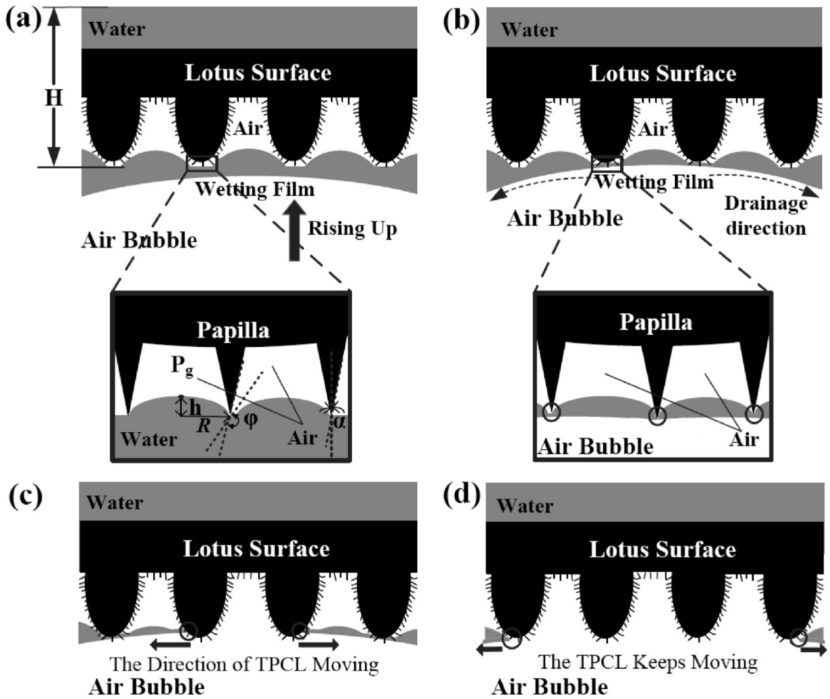


**Figure 6.** Schematic model of air bubble bursting process on lotus leaf surface. (a) A rising air bubble approaching the lotus leaf surface. The foot of (a) is the convex water/air interface formed in nanostructure at equilibrium state. Where $H$ is the height of contact line from the horizontal level, $\varphi$ is the water CA on the smooth surface of the same solid, $\sigma$ is water surface tension, $\alpha$ is the obliquity angle of the asperities surfaces, $\rho$ is the water density, $h$ is the distance between the vertex of convex water/air interface and the asperities, and $R$ is half of the apex spacing between two adjacent micro or nanoasperities. (b) The drainage of the wetting film around the air bubble along the direction shown by the arrows. The foot of (b) shows that the nanobranch-like crystals can penetrate into the water film. (c) When the penetration was deep enough, the nanostructure induces air bubble bursting, and the TPCL forms. Here, the TPCL is the gas/liquid/solid interfaces in the circles, the cross-section view of which is shown by two points. (d) The process of the TPCL moving.

those with more than 170° bubble CA are indicated using the dashed line panes. From Table 1, the height of the microcone array can be seen to significantly affect air bubble bursting. Air bubbles could not burst when the height of microcone array is about 5.0 $\mu$m, regardless of the width or the spacing. For height of approximately 14.5 $\mu$m, or similar to that of the lotus papillae, when the width and spacing, respectively, are about 5−10 $\mu$m and 7−14 $\mu$m, the corresponding bubble CAs were more than 150°, and these cases were considered to be on the verge of bursting, as illustrated in Figure S2d (see Supporting Information). On the other hand, the air bubble did not show bursting characteristics when the width and the spacing were out of this size range. This size and distribution pattern of micro/nano hierarchical rough structures that was effective on air bubble bursting agreed well with the statistical results obtained for lotus papillae (the statistical bottom diameter and spacing of papillae are 7−10 $\mu$m and 5−12 $\mu$m, respectively). Therefore, the hierarchical structures, optimized after a natural long evolution, proved beneficial to air bubble bursting. When the height of the microcone array is 40.0 $\mu$m, most bubble CAs were more than 150° (solid line pane), indicating that the width and spacing exerted only slight influence here. These results strongly suggest that the size and distribution of the microstructure of the lotus leaf played an important role in the air bubble bursting phenomenon.

In order to reveal the influence that the micro/nano hierarchical rough structures of the lotus leaf had on the air bubble bursting effect, an original model was proposed, as shown in Figure 6. Figure 6a presents the schematic illustration of four micropapillae with nanobranch-like crystals, which is immersed in water at a certain distance from the rising air bubble. The depth from the apex of the nanostructure to the horizontal water line is denoted $H$. The thin water film that separates the solid surface from the air bubble is defined as the wetting film, and its stability is controlled by the interfacial interaction forces. Air pockets are captured within the asperities on lotus leaf surface,[36−38] and a convex water/air interface forms between micro and nanostructures (the convex interface in the nanostructure magnified at the foot of Figure 6a). The wetting film gradually becomes thinner as the rising air bubble approaches the leaf surface (Figure 6b). If we consider that a wetting film approaching nanobranch-like crystals would thin more easily, the crystals appeared to penetrate into the rising air bubble when it was close enough to the leaf surface (see the bottom of Figure 6b). The attenuation of the wetting film would finally lead to the coalescence of the air bubble with the captive air pockets among the asperities (Figure 6c), resulting in the formation of TPCL (vertical to the planar surface of paper; see the circles in Figure 6c).[39,40] Once the TPCL formed, the air bubble would spread along the gas bridges between the air bubble and the leaf surface,[41] and the TPCL would be propagated (Figure 6d) until the air bubble had completely spread out.

As for the theoretical evaluation of this mode's validity, the state of the interface between water and the captive air pockets was a decisive factor, which affected the applicability of the air bubble bursting process on the lotus leaf surface. Accordingly,

(36) Ishida, N.; Sakamoto, M.; Miyahara, M.; Higashitani, K. *Langmuir* **2000**, *16*, 5681.
(37) Tyrell, J. W. G.; Attard, P. *Langmuir* **2002**, *18*, 160.
(38) Tyrell, J. W. G.; Attard, P. *Phys. Rev. Lett.* **2001**, *87*, 176104.
(39) Nguyena, A. V.; Stechemesser, H. *Phys. Chem. Chem. Phys.* **2004**, *6*, 429.
(40) Carrier, V.; Colin, A. *Langmuir* **2003**, *19*, 4535.
(41) Ishida, N.; Sakamoto, M.; Miyahara, M.; Higashitani, K. *J. Colloid Interface Sci.* **2002**, *253*, 112.

silvery layers of air films trapped on lotus leaf surfaces were observed, and it was found that, when the lotus leaf was immerged into water, silvery layers of air films could be trapped on it, but it was not homogeneous and stable. After immersing for 30 min, air transported among papillae and over the lotus leaf surface to form a well-proportioned air film, which could be stable for more than 3 h (see Figure S1 in Supporting Information). Therefore, all the samples had been immersed in the experimental apparatus for at least 30 min before testing to achieve a redistributed well-proportioned air layer in water. Besides, it was noticeable that the water environment was connected to the atmospheric air and it was saturated with air, so depletion of the air film by dissolution in water did not happen obviously during the stable state. It was reasonable to believe that all the investigated superhydrophobic surfaces reached the equilibrium state of the interface between water and the captive air pockets. On the basis of the Tsori's equation for capillaries with height-dependent cross-section at the quasi-static condition (the equilibrium state)[42] and the Laplace-Young's equation,[43] the Laplace pressure at the contact line TPCL in the above model could be deduced as follows:

$$P_g + \frac{2\sigma \cos(\varphi+\alpha)}{R+h \tan\alpha} + \rho g h = P_o + \rho g H \qquad (1)$$

where $P_g$ is the pressure in the captive air pockets, $P_o$ is the atmospheric pressure, $\varphi$ is water CA on smooth surface of the same solid, $\sigma$ is water surface tension, $\alpha$ is obliquity angle of the asperity surfaces, $\rho$ is water density, $h$ is the distance between the vertex of convex water/air interface and the asperities, and $R$ is half of the apex spacing between two adjacent micro or nanoasperities. Herein, $R$ is a parameter that is determined by the different scale of asperities, so $R_{micro}$ is much larger than $R_{nano}$.

The pressure difference ($\Delta P$) between $P_g$ and $P_o$ among the asperities with obliquity angle of $\alpha$ could be described by

$$\Delta P = P_g - P_o = \rho g(H-h) - \frac{2\sigma \cos(\varphi+\alpha)}{R+h \tan\alpha} \qquad (2)$$

Since the captive air pockets among asperities are microscopic or nanoscopic, $H$ is much larger than $h$, so $\Delta P$ could be approximately calculated as

$$\Delta P = \rho g H - \frac{2\sigma \cos(\varphi+\alpha)}{R+h \tan\alpha} \qquad (3)$$

The value of $\varphi$ is larger than 90° as measured by the primary component of epicuticular wax[44] and $\alpha$ is less than 90°, so the sum of $\varphi$ and $\alpha$ ranges 90−270°, and $\cos(\varphi + \alpha)$ is less than zero. Hence, $\Delta P$ is larger than zero, and the Laplace pressure of the captive air pockets is larger than the atmospheric pressure. Consequently, once an air bubble approached the asperities, coalescence would occur between the air bubble and the captive air pockets. $R_{micro}$ is much larger than $R_{nano}$, so $\Delta P_{micro}$ is smaller than $\Delta P_{nano}$, which indicates that the coalescence in the nanostructure was easier than that in microstructure, i.e., nanostructure could accelerate air bubble bursting. Therefore, the air bubble were seen to burst faster on the lotus leaf and the "artificial lotus leaf" due to their combination of micro/nanohierarchical rough structures. In addition, it was assumed that the surfaces that contained only nanostructures would have insufficient space to form gas bridges for air bubble spreading; thus, none was seen.

(42) Tsori, Y. *Langmuir* **2006**, *22*, 8860.
(43) de Gennes, P.; Brochard-Wyart, F.; Quéué, D. *Capillarity and wetting phenomena: drops, bubbles, pearls, waves*; Springer: New York, 2004; Chapter 2.
(44) Barthlott, W.; Neinhuis, C.; Cutler, D.; Ditsch, F.; Meusel, I.; Theisen, I.; Wilhelmi, H. *Bot. J. Linn. Soc.* **1998**, *126*, 237.

## Conclusions

In summary, a novel phenomenon of air bubble bursting on a lotus leaf surface was discovered and the underlying mechanism was attributed to the micro/nano hierarchical rough structures. Air pockets captured in the nanostructure of the lotus leaf could easily coalesce with the air bubble, and the microstructure could provide enough space to form gas bridges for air bubble spreading. Thus, the combination of nano and microstructure was responsible for the air bubble bursting effect on the superhydrophobic surfaces consisting of micro/nano hierarchical structures. Moreover, the size and distribution of the microstructure of the lotus leaf played important roles in the air bubble bursting process. A superhydrophobic "artificial lotus leaf", which mimicked the micro/nano hierarchical rough structures of the lotus leaf, was constructed and also created a similar air bubble bursting effect. This bursting effect induced on superhydrophobic surfaces with micro/nano hierarchical rough structures should spark further theoretical study of other bubble-related interfacial phenomena. From a practical standpoint, it may also find wide application in industrial separation processes, such as mineral flotation, food processing, textile dyeing, and fermentation, without the requirement for any accessional energy or other additives.

**Acknowledgment.** The authors thank the State Key Project Fundamental Research (2007CB936403), the National Nature Science Foundation of China (20125102, 90306011), and the Innovation Foundation of the Chinese Academy of Sciences for the continuing financial support. Also, thanks to Dr. Yizhuo Gu for helpful discussions and suggestions.

**Supporting Information Available:** Microscope photographs of silvery layers of air films on the lotus leaf surface at different immersion time, and a typical series of optical images showing air bubbles final state and their air bubble CAs on four kinds of superhydrophobic surfaces. This material is available free of charge via the Internet at http://pubs.acs.org.